

Synthesis and Mesomorphic Properties of Rigid-Core Ionic Liquid Crystals

Paul H. J. Kouwer[‡] and Timothy M. Swager*

Contribution from the Department of Chemistry, Massachusetts Institute of Technology,
77 Massachusetts Avenue, Cambridge, Massachusetts 02139

Received July 28, 2007; E-mail: tswager@mit.edu

Abstract: Ionic liquid crystals combine the unique solvent properties of ionic liquids with self-organization found for liquid crystals. We report a detailed analysis of the structure–property relationship of a series of new imidazolium-based liquid crystals with an extended aromatic core. Investigated parameters include length and nature of the tails, the length of the rigid core, the lateral substitution pattern, and the nature of the counterion. Depending on the molecular structure, two mesophases were observed: a bilayered SmA₂ phase and the more common monolayered SmA phase, both strongly interdigitated. Most materials show mesophases stable to high temperatures. For some cases, crystallization could be suppressed, and room-temperature liquid crystalline phases were obtained. The mesomorphic properties of several mixtures of ionic liquid crystals were investigated. Many mixtures showed full miscibility and ideal mixing behavior; however, in some instances we observed, surprisingly, complete demixing of the component SmA phases. The ionic liquid crystals and mixtures presented have potential applications, due to their low melting temperatures, wide temperature ranges, and stability with extra ion-doping.

Introduction

Over the past decade ionic liquids (ILs) have become a mature class of materials with applications as reaction media for organic synthesis. Initial interest developed from the fact that ILs eliminate the hazards associated with harmful and volatile conventional solvents. Currently, many ILs can be categorized as “task-specific” ionic liquids (TSIL), in which one or more functionalities have been added to their primary role as solvent.¹ For example, TSILs may show catalytic activity,² function as a ligand^{1a} or as a solvent in chemical synthesis.³ Other important emerging fields of application are in separation and extraction processes,⁴ in the synthesis⁵ and functionalization⁶ of nanosized

materials, and as electrochemical components in various devices, such as lithium ion batteries, fuel cells, solar cells, and capacitors.⁷

Liquid crystals (LCs) offer the combination of order and mobility in one material. When LC molecules only possess orientational order, a nematic phase is observed. In a smectic LC phase, the molecules show one-dimensional positional order, resulting in a layered phase. The lowest-symmetry layered phase is the smectic A (SmA) phase, with the average orientation of the mesogen long axis normal to the layers. In a smectic C (SmC) phase the molecules are tilted with respect to the layer normal. Higher-ordered smectic phases have some degree of in-plane and/or between-planes positional order, and many of these phases are considered crystal or soft-crystal phases.

The unique properties liquid crystals offer have led to their widespread application in display technology; however, many other applications in a variety of fields are currently suggested and investigated. One of those applications is the use of LCs as a templating medium. Some examples are the alignment of polymers⁸ or chromophores⁹ and controlled metal deposition or nanoparticle synthesis.¹⁰

The merger of ILs and LCs has yielded a new class of materials called ionic liquid crystals (ILCs). These self-

[‡] Current address: Radboud University, Institute for Molecules and Materials, Toernooiveld 1, 6525 ED Nijmegen, The Netherlands. E-mail: kouwer@science.ru.nl

- (1) For recent reviews on task-specific ionic liquids: (a) Lee, S. *Chem. Commun.* **2006**, 1049–1063. (b) Davis, J. D., Jr. Synthesis of task-specific ionic liquids. In *Ionic Liquids in Synthesis*; Wasserscheid, P., Welton, T., Eds.; Wiley-VCH: Berlin, 2003; pp 33–40.
- (2) For examples of Friedel-Crafts reactions: (a) Boon, J. A.; Levisky, J. A.; Pflug, J. L.; Wilkes, J. S. *J. Org. Chem.* **1986**, *51*, 480. Esterifications: (b) Cole, A. C.; Jensen, J. L.; Ntai, I.; Tran, K. L. T.; Weaver, K. J.; Forbes, D. C.; Davis, J. H. *J. Am. Chem. Soc.* **2002**, *124*, 5962–5963.
- (3) (a) Fraga-Dubreuil, J.; Bazureau, J. P. *Tetrahedron Lett.* **2001**, *42*, 6097–6100. (b) Miao, W.; Chan, T. H. *Org. Lett.* **2003**, *5*, 5003–5005. (c) Anjaiah, S.; Chandrasekhar, S.; Gree, R. *Tetrahedron Lett.* **2004**, *45*, 569–571.
- (4) (a) Visser, A. E.; Swatloski, R. P.; Reichert, W. M.; Davis, J. H.; Rogers, R. D.; Mayton, R.; Sheff, S.; Wierzbicki, A. *Chem. Commun.* **2001**, 135–136. (b) Visser, A. E.; Swatloski, R. P.; Reichert, W. M.; Mayton, R.; Sheff, S.; Wierzbicki, A.; Davis, J. H.; Rogers, R. D. *Environ. Sci. Technol.* **2002**, *36*, 2523–2529.
- (5) (a) Gadenne, B.; Hesemann, P.; Moreau, J. J. E. *Chem. Commun.* **2004**, 1768–1769. (b) Dobbs, W.; Suisse, J.-M.; Douce, L.; Welter, R. *Angew. Chem., Int. Ed.* **2006**, *45*, 4179–4182. (c) Zhu, Y. J.; Wang, W. W.; Qi, R. J.; Hu, X. L. *Angew. Chem., Int. Ed.* **2004**, *43*, 1410. (d) Wang, Y.; Yang, H. *J. Am. Chem. Soc.* **2005**, *127*, 5316.

- (6) (a) Itoh, H.; Naka, K.; Chujo, Y. *J. Am. Chem. Soc.* **2004**, *126*, 3026–3027. (b) Kim, K.-S.; Demberelnyamba, D.; Lee, H. *Langmuir* **2004**, *20*, 556–560.

- (7) (a) Trulove, P. C.; Mantz, R. A. Electrochemical Properties of Ionic Liquids. In *Ionic Liquids in Synthesis*; Wasserscheid, P., Welton, T., Eds.; Wiley-VCH: Berlin, 2003; pp 103–126. (b) Ohno, H., Ed. *Electrochemical Aspects of Ionic Liquids*; Wiley: Hoboken, NJ, 2005. (c) Buzzee, M. C.; Evans, R. G.; Compton, R. G. *ChemPhysChem* **2004**, *5*, 1106–1120. (d) Bonhôte, P.; Dias, A.-P.; Papageorgiou, N.; Kalyanasundaram, K.; Grätzel, M. *Inorg. Chem.* **1996**, *35*, 1168–1178. (e) Forsyth, S. A.; Pringle, J. M.; MacFarlane, D. R. *Aust. J. Chem.* **2004**, *57*, 113–119.

organizing systems offer great advantages over isotropic systems. For instance, ion conduction was enhanced in the SmA and columnar phases compared to that in the isotropic phase.¹¹ ILCs have also been used as an anisotropic medium for electrochemistry, where the ILC acted as the solvent, the electrolyte, and the template. Applications in dye-sensitized solar cells have been proposed for these systems.¹² Other efforts have reported the polymerization of conducting polymers in lyotropic phase,¹³ although the latter was a multicomponent system, to which a common electrolyte was added.

Beginning in the late 1980s, an increasing number of reports on ILCs have appeared in the literature. Early papers focused on the mesomorphic properties of small aromatic systems (imidazolium, pyridinium, etc.), substituted by one or multiple long aliphatic tails.¹⁴ The SmA phase displayed by such systems often requires a minimum length of the tail (usually C₁₂), and the observed mesophases strongly depend on the counterion. Replacement of one tail with a threefold substituted benzyl group gives a wedge-shaped ILC that forms columnar (Col) mesophases.^{11b,c} In these types of imidazolium- and pyridinium-based materials, the liquid crystalline properties originate from their strong amphiphilic character. Excluded volume effects induced by a rigid anisotropic molecular core, which are one of the main driving forces for mesophase formation in conventional liquid crystals, play no significant role. As a result, no nematic mesophases can be expected from such systems.

More recently, ILCs have been described in the literature with a conventional liquid crystal mesogen linked via a flexible linker to a conventional ionic liquid, most commonly a 1-methylimidazolium (MIm) group. MIm groups attached to rod-shaped LCs have yielded SmA and SmE phases, even when the liquid crystal used was a strong nematogen.¹⁵ When multiple MIm groups were attached on the tail ends of discotic liquid crystals, stabilized columnar phases were observed.¹⁶ The architecture of these molecules is unconventional, as the imidazolium group is a polarizable rigid group that is suitable as part of a mesogenic core rather than being placed at the ends of flexible tails. To

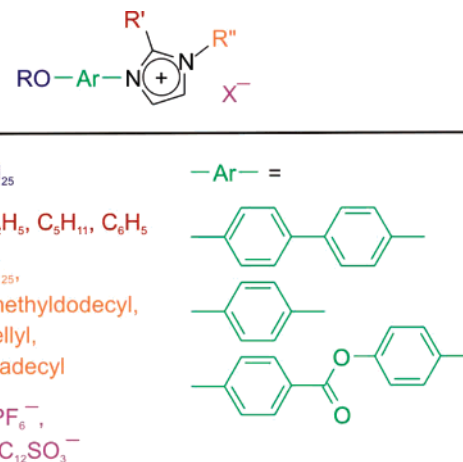


Figure 1. Generic structure of the prepared series of ILCs with different parameters. A total of 47 molecules have been prepared.

date, few mesogens have been described where charged imidazolium groups are incorporated in the rigid core of the mesogen.¹⁷

We report herein a series of ILCs that bridge the classes of ILs and LCs. Through recent developments in aromatic amination chemistry,¹⁸ we were able to conveniently integrate imidazolium groups in the core of the mesogen, which now has the shape of a conventional rod-shaped mesogen. The molecular structures have implications for the organization in the material, and the extended aromatic core increases the order parameter in the LC phase.

A wide variety of parameters were examined for their influence on the mesomorphic properties (Figure 1). These include the tail structure (length, branching, chirality, position), core size, lateral substituents, and counterion. The liquid crystalline properties have been investigated by optical polarizing microscopy (OPM), differential scanning calorimetry (DSC), and X-ray diffraction (XRD). Our conclusions are supported by molecular modeling experiments.

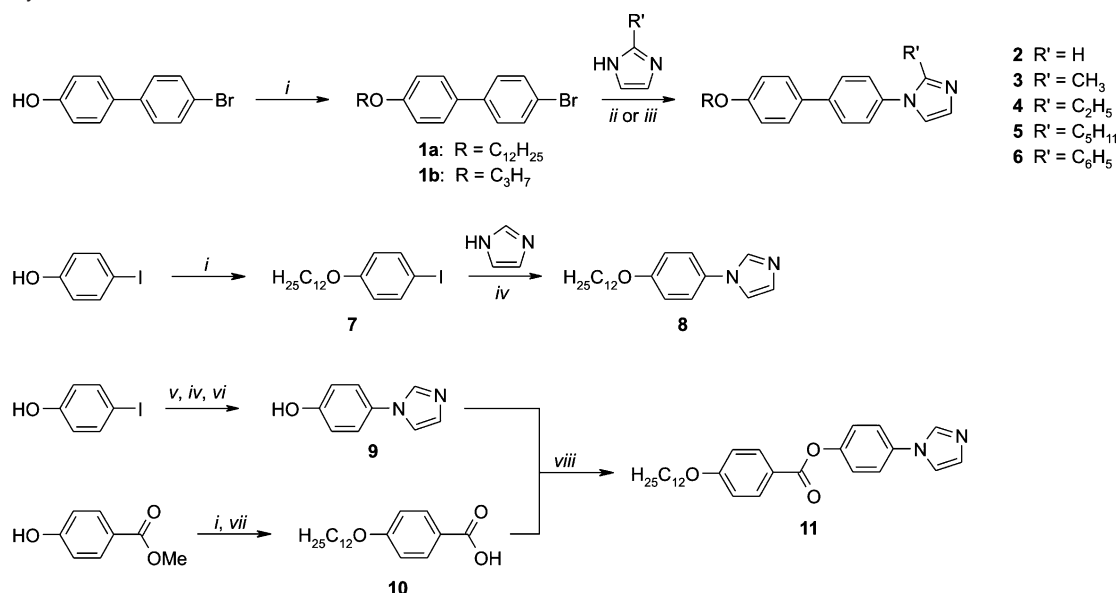
Results and Discussion

Experimental. The synthesis and chemical characterization (¹H, ¹³C NMR) of compounds **1–36** are described in the Supporting Information. After purification by crystallization and/or column chromatography, the materials were dissolved, filtered (0.2 μm pores), and then dried for at least 24 h in vacuum before analysis. Mixtures of different ILCs were prepared by dissolving the appropriate amounts of ILC in a common solvent, which was then removed by evaporation. Mixtures were dried for 24 h under vacuum prior to analysis. ILCs with relatively hydrophobic counterions did not show different phase behavior after exposure to atmospheric conditions.

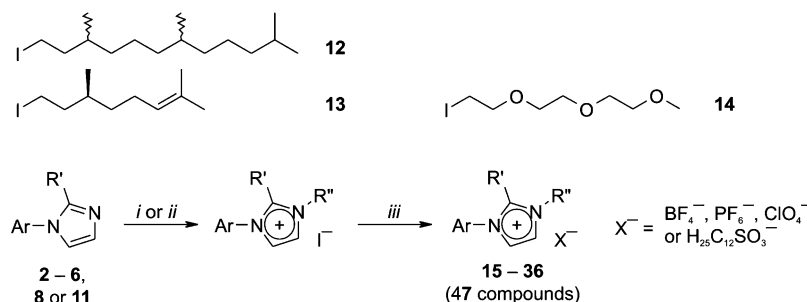
Synthesis. The synthesis of the ILCs studied is outlined in Schemes 1 and 2. Alkoxy-tails were introduced at the far end of the mesogen under standard Williamson etherification conditions. To prepare **9**, the phenol group was protected with a tetrahydropyranyl group. However, it was recently published

- (8) Zhu, Z.; Swager, T. M. *J. Am. Chem. Soc.* **2002**, *124*, 9670–9671.
- (9) (a) Long, T. M.; Swager, T. M. *Adv. Mater.* **2001**, *13*, 601–604. (b) Long, T. M.; Swager, T. M. *J. Am. Chem. Soc.* **2002**, *124*, 3826–3827. (c) Amemiya, K.; Shin, K. C.; Takanishi, Y.; Ishikawa, K.; Azumi, R.; Takezoe, H. *J. Appl. Phys.* **2004**, *43*, 6084–6087.
- (10) (a) Gray, D. H.; Gin, D. L. *Chem. Mater.* **1998**, *10*, 1827. (b) Dag, Ö.; Alayoglu, S.; Tura, C.; Celik, Ö. *Chem. Mater.* **2003**, *15*, 2711–2717. (c) Yamauchi, Y.; Momma, T.; Yokoshima, T.; Kuroda, K.; Osaka, T. *J. Mater. Chem.* **2005**, *15*, 1987–1994.
- (11) (a) Hoshino, K.; Yoshio, M.; Mukai, T.; Kishimoto, K.; Ohno, H.; Kato, T. *J. Polym. Sci., Part A: Polym. Chem.* **2003**, *41*, 3486–3492. (b) Yoshio, M.; Mukai, T.; Ohno, H.; Kato, T. *J. Am. Chem. Soc.* **2004**, *126*, 994–995. (c) Yoshio, M.; Kagata, T.; Hoshino, K.; Mukai, T.; Ohno, H.; Kato, T. *J. Am. Chem. Soc.* **2006**, *128*, 5570–5577.
- (12) Yamanaka, N.; Kawano, R.; Kubo, W.; Kitamura, T.; Wada, T.; Watanabe, M.; Yanagida, S. *Chem. Commun.* **2005**, 740–742.
- (13) (a) Hulvat, J. F.; Stupp, S. I. *Angew. Chem., Int. Ed.* **2003**, *42*, 778. (b) Hulvat, J. F.; Stupp, S. I. *Adv. Mater.* **2004**, *16*, 589–592.
- (14) (a) Bowlas, C. J.; Bruce, D. W.; Seddon, K. R. *Chem. Commun.* **1996**, 1625. (b) Gordon, C. M.; Holbrey, J. D.; Kennedy, A. R.; Seddon, K. R. *J. Mater. Chem.* **1998**, *8*, 2627. (c) Holbrey, J. D.; Seddon, K. R. *J. Chem. Soc., Dalton Trans.* **1999**, 2133. (d) Tosoni, M.; Laschat, S.; Baro, A. *Helv. Chim. Acta* **2004**, *87*, 2742. (e) Knight, G. A.; Shaw, B. D. *J. Chem. Soc.* **1938**, 682. (f) Sudholter, E. J. R.; Engberts, J. B. F. N.; de Jeu, W. J. *Phys. Chem.* **1982**, *86*, 1908.
- (15) For example: (a) Hoshino, K.; Yoshio, M.; Mukai, T.; Kishimoto, K.; Ohno, H.; Kato, T. *J. Polym. Sci., Part A: Polym. Chem.* **2003**, *41*, 3486. (b) Navarro-Rodriguez, D.; Frere, Y.; Gramain, P.; Guillon, D.; Skoulios, A. *Liq. Cryst.* **1991**, *9*, 321. (c) Cui, L.; Sapagovas, V.; Lattermann, G. *Liq. Cryst.* **2002**, *29*, 1121. (d) Yoshizawa, H.; Mihara; Koide, N. *Mol. Cryst. Liq. Cryst.* **2004**, *423*, 61. (e) El Hamaoui, B.; Zhi, L.; Pisula, W.; Kolb, U.; Wu, J.; Müllen, K. *Chem. Commun.* **2007**, 2384.
- (16) Motoyanagi, J.; Fukushima, T.; Aida, T. *Chem. Commun.* **2005**, 101.

- (17) (a) Kosaka, Y.; Kato, T.; Uryu, T. *Liq. Cryst.* **1995**, *18*, 693–698. (b) Suisse, J. M.; Bellemin-Lapontaz, S.; Douce, L.; Maisse-Francois, A.; Welter, R. *Tetrahedron Lett.* **2005**, *46*, 4303–4305.
- (18) (a) Altman, R. A.; Buchwald, S. L. *Org. Lett.* **2006**, *8*, 2779–2782. (b) Zhang, H.; Cai, Q.; Ma, D. *J. Org. Chem.* **2005**, *70*, 5164–5173. (c) Ma, D.; Cai, Q.; Zhang, H. *Org. Lett.* **2003**, *5*, 2453.

Scheme 1. Synthesis of the ILC Precursors^a

^a Key: (i) RBr, K₂CO₃, KI, butanone, 16 h reflux; (ii) K₂CO₃, CuI, *N,N*-dimethylglycine, DMSO, 24–48 h at 110 °C; (iii) Ce₂CO₃, CuI, 4,7-dimethoxy-1,10-phenanthroline, PEG-600, butyronitril 4–24 h reflux; (iv) K₂CO₃, CuI, L-proline, DMSO, 16 h at 110 °C; (v) tetrahydropyran, *p*-toluenesulfonic acid, CH₂Cl₂, 2 h at room temperature; (vi) MeOH, 1 N HCl, 2 h at room temperature; (vii) (a) 5N KOH, EtOH, 2 h reflux; (b) concd HCl to neutral; (viii) 1,3-dicyclohexylcarbodiimide (DCC); 4-(*N,N*-dimethylamino)pyridine (DMAP), THF, 40 h at 50 °C.

Scheme 2. Synthesis of the ILCs^a

^a Key: (i) Propyl or dodecyl iodide, neat, 4–24 h at 100 °C; (ii) **12**, **13**, or **14**, toluene, 16–40 h at 100 °C; (iii) ion exchange: BF₄[−] and PF₆[−] by multiple washes with concentrated aqueous NaBF₄ or NH₄PF₆ solutions, respectively; ClO₄[−] through a AgClO₄ solution; H₂₅C₁₂SO₃[−] (dodecylsulfonate) through prefunctionalized beads.

that imidazole can be coupled directly to 4-iodophenol in an excellent yield.^{18a}

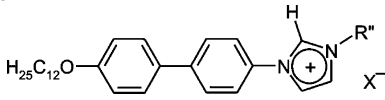
The key step in the synthesis was an Ullman-type coupling of an aryl iodide or bromide with imidazole and 2-substituted imidazole derivatives. Recent literature shows that the copper-catalyzed reaction can be facilitated by the use of specific ligands, which makes this type of reaction a particularly useful tool in the formation of aryl heterocyclic compounds.¹⁸ The procedures described by Ma et al.^{18b,c} were used for unsubstituted imidazoles. In their work, they describe good to excellent yields with commercially available, inexpensive ligands. The reactions are relatively slow, but minimal byproducts are produced, and any unreacted arylhalide is easily recovered in the purification procedure. For 2-alkyl- or 2-phenyl-substituted imidazoles, these reaction conditions gave low conversions, and the dimethoxyphenanthroline ligand following the methods of Buchwald et al. gave superior results.^{18a} Under Buchwald's conditions, we were able to obtain moderate yields for imidazoles with bulky substituents (pentyl and phenyl) at the 2-position.¹⁹

The alkylation of 1-arylimidazoles needed optimization, and we found that alkyl iodides are required to give full conversion under reasonable conditions. Therefore, the (commercially) available alkyl bromides and the tosylates²⁰ were converted into iodides **12–14** by means of Finkelstein-type reactions. The alkylations with alkyl iodides were conducted either without any solvent (*n*-propyl iodide and *n*-dodecyl iodide) or in toluene solution. The reduced concentration when a solvent is used generally leads to longer reaction times. After the alkylation reaction, pure products were obtained by multiple crystallizations, if necessary preceded by column chromatography. Iodide ions were exchanged by multiple washings of a dichloromethane solution of the ILC with concentrated aqueous sodium salt solutions (BF₄[−] and PF₆[−]), by precipitation of silver iodide (using AgClO₄), or by treatment with pre-functionalized beads (sulfonates). Tables 1 and 2 show the variation in the materials that were prepared.

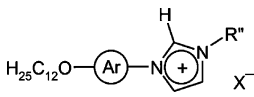
Mesomorphic Properties. To systematically investigate the influence of specific chemical parameters on the mesophase behavior, we will discuss the materials in separate series in

(19) Note that for reactions with the bulky 2-phenylimidazole, we were not able to obtain the high yields reported in literature (ref 18a).

(20) Jullien, L.; Canceill, J.; Lacombe, L.; Lehn, J. M. *J. Chem. Soc., Perkins Trans. 2* **1995**, 417–426.

Table 1. Prepared ILCs with Yields of the Alkylation Step and the Ion Exchange


mesogen	R'' ^a	X ⁻	y/%
15a	<i>n</i> -C ₃ H ₇	I ⁻	92
15b	<i>n</i> -C ₃ H ₇	BF ₄ ⁻	97
15c	<i>n</i> -C ₃ H ₇	PF ₆ ⁻	98
15d	<i>n</i> -C ₃ H ₇	ClO ₄ ⁻	88
15e	<i>n</i> -C ₃ H ₇	H ₂₅ C ₁₂ SO ₃ ⁻	71
16a	<i>n</i> -C ₁₂ H ₂₅	I ⁻	86
16b	<i>n</i> -C ₁₂ H ₂₅	BF ₄ ⁻	98
17a	TMD	I ⁻	84
17b	TMD	BF ₄ ⁻	98
18a	<i>S</i> -citronellyl	I ⁻	91
18b	<i>S</i> -citronellyl	BF ₄ ⁻	96
19a	Me(OCH ₂ CH ₂) ₃ ⁻	I ⁻	70
19b	Me(OCH ₂ CH ₂) ₃ ⁻	BF ₄ ⁻	92



mesogen	Ar	R'' ^a	X ⁻	y/%
20a	PhCO ₂ Ph	<i>n</i> -C ₃ H ₇	I ⁻	89
20b	PhCO ₂ Ph	<i>n</i> -C ₃ H ₇	BF ₄ ⁻	95
21a	PhCO ₂ Ph	<i>n</i> -C ₁₂ H ₂₅	I ⁻	92
21b	PhCO ₂ Ph	<i>n</i> -C ₁₂ H ₂₅	BF ₄ ⁻	94
22a	PhCO ₂ Ph	TMD	I ⁻	90
22b	PhCO ₂ Ph	TMD	BF ₄ ⁻	96
23a	Ph	<i>n</i> -C ₃ H ₇	I ⁻	65
24a	Ph	<i>n</i> -C ₁₂ H ₂₅	I ⁻	78
24b	Ph	<i>n</i> -C ₁₂ H ₂₅	BF ₄ ⁻	87
25a	Ph	TMD	I ⁻	75
25b	Ph	TMD	BF ₄ ⁻	90

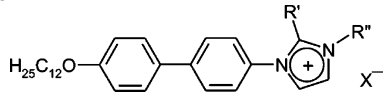
^a TMD = 3,7,11-trimethyldodecyl; *S*-DMO = *S*-3,7-dimethyloctyl; Me(OCH₂CH₂)₃⁻ = 3,6,9-trioxadecyl.

which only one structural element is varied. Compounds **15** and **16** have been used as “internal standards” in all series. Tables with the mesomorphic properties and XRD results of all synthesized materials are included in the Supporting Information.²¹

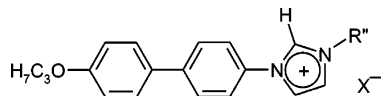
OPM analysis of the LC samples consistently showed the characteristic focal conical textures of a SmA phase (Figure 2a). The textures are often combined with large spontaneous homeotropically aligned areas that are optically isotropic when viewed normal to the glass surfaces, particularly on cooling from the isotropic phase, even between unprepared glass slides (Figure 2b). At lower temperature, crystal and soft crystal phases are observed. Optical textures of these lower temperature phases, shown in Figure 2c,d, are not conclusive, and no attempt has been made to further elucidate their identity.

DSC measurements were performed on all liquid crystalline materials and mixtures. Transition temperatures were recorded as the local maxima of the endotherm. Five characteristic examples are shown in Figure 3. Generally, the DSC traces were simple and showed two transitions, the melting and the clearing point. Some materials showed suppression of crystallization. In the first heating, the solid, as obtained from the synthesis, shows a clear melting transition. However, the reverse process is not observed in the cooling run. Instead, a glass transition is observed around room temperature. In the second heating run,

(21) Note that more ionic liquid crystals have been synthesized than discussed in the body of the paper. All synthesized materials are in the Supporting Information.

Table 2. Prepared ILCs with Yields of the Alkylation Step and the Ion Exchange


mesogen	R'	R''	X ⁻	y/%
26a	CH ₃	<i>n</i> -C ₃ H ₇	I ⁻	92
26b	CH ₃	<i>n</i> -C ₃ H ₇	BF ₄ ⁻	92
27a	CH ₃	<i>n</i> -C ₁₂ H ₂₅	I ⁻	90
27b	CH ₃	<i>n</i> -C ₁₂ H ₂₅	BF ₄ ⁻	93
28a	C ₂ H ₅	<i>n</i> -C ₃ H ₇	I ⁻	87
28b	C ₂ H ₅	<i>n</i> -C ₃ H ₇	BF ₄ ⁻	97
29a	C ₂ H ₅	<i>n</i> -C ₁₂ H ₂₅	I ⁻	82
29b	C ₂ H ₅	<i>n</i> -C ₁₂ H ₂₅	BF ₄ ⁻	97
30a	C ₅ H ₁₁	<i>n</i> -C ₃ H ₇	I ⁻	83
30b	C ₅ H ₁₁	<i>n</i> -C ₃ H ₇	BF ₄ ⁻	98
31a	C ₅ H ₁₁	<i>n</i> -C ₁₂ H ₂₅	I ⁻	76
31b	C ₅ H ₁₁	<i>n</i> -C ₁₂ H ₂₅	BF ₄ ⁻	93
32a	Ph	<i>n</i> -C ₁₂ H ₂₅	I ⁻	67
32b	Ph	<i>n</i> -C ₁₂ H ₂₅	BF ₄ ⁻	72



mesogen	R'' ^a	X ⁻	y/%
33a	<i>n</i> -C ₃ H ₇	I ⁻	80
33e	<i>n</i> -C ₃ H ₇	H ₂₅ C ₁₂ SO ₃ ⁻	52
34a	<i>n</i> -C ₁₂ H ₂₅	I ⁻	90
34b	<i>n</i> -C ₁₂ H ₂₅	BF ₄ ⁻	96
35e	<i>n</i> -C ₁₂ H ₂₅	H ₂₅ C ₁₂ SO ₃ ⁻	62
35a	TMD	I ⁻	92
35b	TMD	BF ₄ ⁻	93
36a	Me(OCH ₂ CH ₂) ₃ ⁻	I ⁻	59
36b	Me(OCH ₂ CH ₂) ₃ ⁻	BF ₄ ⁻	67

^a TMD = 3,7,11-trimethyldodecyl; Me(OCH₂CH₂)₃⁻ = 3,6,9-trioxadecyl.

some materials show a cold crystallization process preceding the melting transition (for instance **15c**), whereas in others, no crystallization is observed (for instance **20b**). Because the glass transition temperatures are generally around room temperature, the SmA phase of the latter group shows an unusually broad temperature window, which is beneficial for applications. The supercooled state of the latter materials is stable for months. Some materials in the series displayed crystal polymorphism (e.g., traces **18b** and **21b**). At lower temperatures, multiple transitions, probably (soft) crystal–crystal transitions, are visible in the DSC traces. Compound **22a** shows three such transitions before melting into the SmA phase. Some laterally substituted ILCs show transitions to another smectic phase on decreasing temperatures.

X-ray diffraction studies in the mesophase show the characteristic SmA pattern with a strong fundamental (001) reflection, a small first order (002) reflection, and a diffuse reflection of the alkyl tails around 4.5 Å (Figure 4). Typically, in the (soft) crystal phases at lower temperatures, the layered organization is conserved. The presence of sharper reflections at lower temperatures in the wide angle region indicates the increased order within the layers of these phases.

The (001) reflections were fit with a Gaussian distribution to obtain the layer spacings d_{001} over a wide temperature range (see the inset in Figure 4). Depending on the alkyl substitution pattern of the ILC, the molecules organize either in monolayers SmA_d with $d_{001} < L_{\text{calc}}$, or in bilayers SmA₂ with $L_{\text{calc}} < d_{001}$

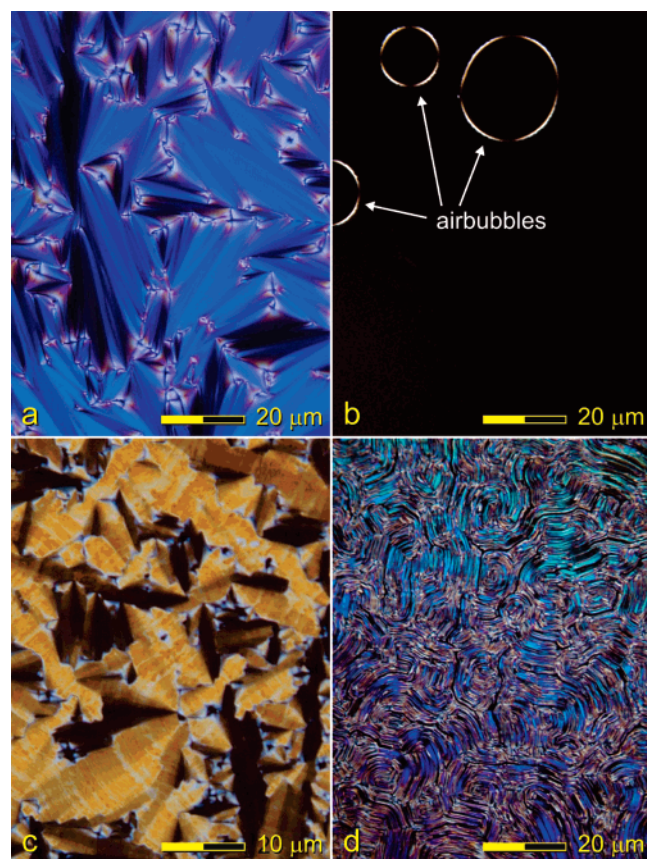


Figure 2. Optical polarizing microscopy images: (a) **24b** at $T = 130$ °C (focal conic SmA phase); (b) **15e** at $T = 178$ °C; (c) **22a** at $T = 182$ °C (CrZ phase); (d) **24b** at $T = 50$ °C (CrX phase). All pictures are taken with crossed polarizers. The scale-bar is shown in the figures.

$< 2 L_{\text{calc}}$, where L_{calc} is the molecular length of the fully extended mesogens with the aliphatic tails in an all-trans configuration. Hence, the experimentally determined molecular length L_{XRD} equals the layer spacing d_{001} for monolayered materials and equals half of the layer spacing in the case of bilayers.

Molecular modeling studies (Supporting Information) suggest that the long axis of the mesogens is considerably larger than the experimental layer thickness in the SmA phase, which indicates that the aliphatic tails are strongly interdigitated. To quantify the extent of interdigitation the ratio $L_{\text{XRD}}/L_{\text{calc}}$ was calculated. Since the layer spacing in many materials is strongly dependent on the temperature, L_{XRD} was determined at reduced temperature $T = 0.95 T_{\text{Iso}}$. ILC **17b** is an indicative example (Figure 4) with $L_{\text{calc}} = 41.2$ Å and $L_{\text{XRD}} = 30.9$ Å; the flexible tails are largely interdigitated at this temperature. The interdigitation is likely the result of an increased effective volume of the mesogen core due to the presence of the counterion.

All of SmA layer spacings display a strong linear temperature dependence ($d_{001} = \alpha + \beta T$). Interestingly, **17b**, L_{XRD} extrapolated to $T = 0$ K gives a value of 42.5 Å, which is close to the calculated value of 41.2 Å. An analysis of the temperature dependence and the interdigitation of the different series of materials will be discussed later. The layer spacings of the crystal phase(s) were either similar to the SmA phase or smaller with a continued reduction in length with decreasing temperature. The example shown in Figure 4 indicates a tilt of the mesogens in the layers below the SmA phase, although no (soft) crystal phase assignments have been made from X-ray patterns.

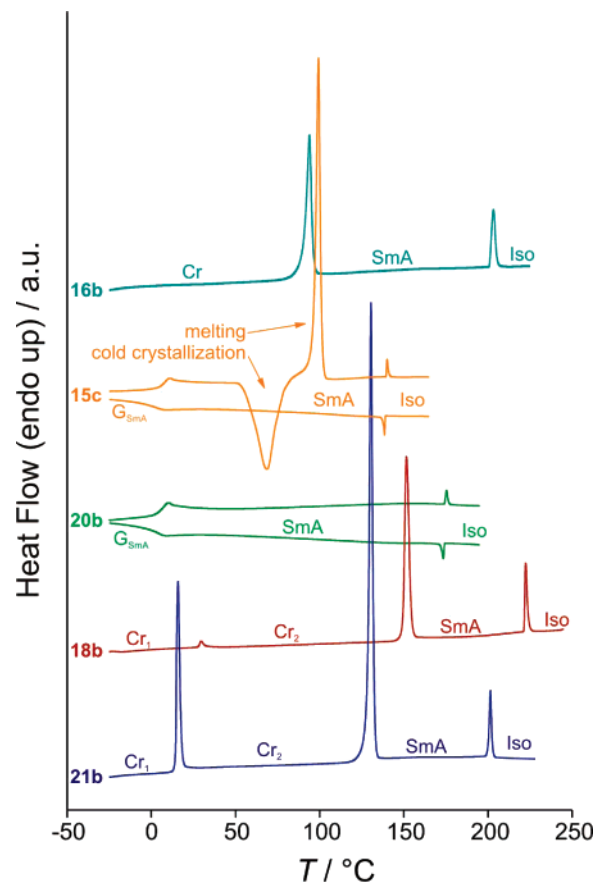


Figure 3. Normalized DSC traces of selected mesogens: **16b**, characteristic trace of an ILC; **15c**, suppression of crystallization with cold crystallization; **20b** complete suppression of crystallization; **18b** and **21b** polymorphism at lower temperatures. All traces are second heating runs and first cooling runs. Third cooling runs were identical to the second, provided that no degradation took place ($T > 230$ °C).

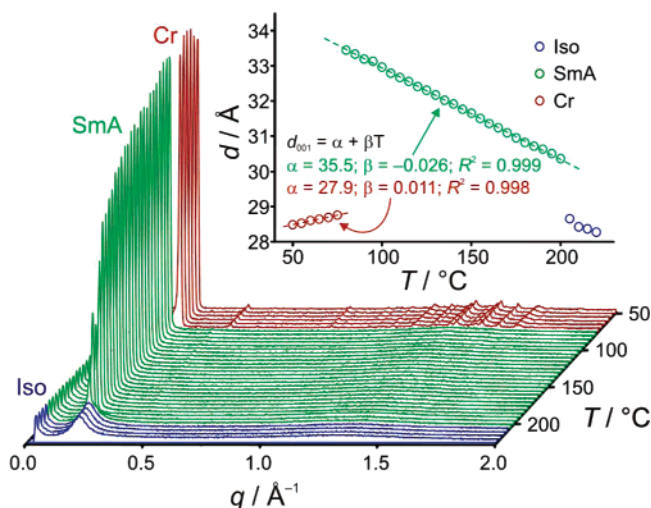


Figure 4. XRD results from **17b**, recorded cooling from the isotropic phase (diffractograms every 5 °C recorded with exposure times of 10 min per measurement). (Inset) Temperature dependence of the layer spacing. The dashed lines are linear fits of the SmA phase and the soft crystal phase. Fitting results (°C) are indicated in the figure.

Series 1. Evaluation of the Influence of the N-Alkyl Substituent. We investigated ILCs by first modifying the length of the aliphatic tails. Shorter tails generally give higher clearing temperatures and mesophases with no positional order (i.e., nematic phases). Increasing the tail length initially reduces

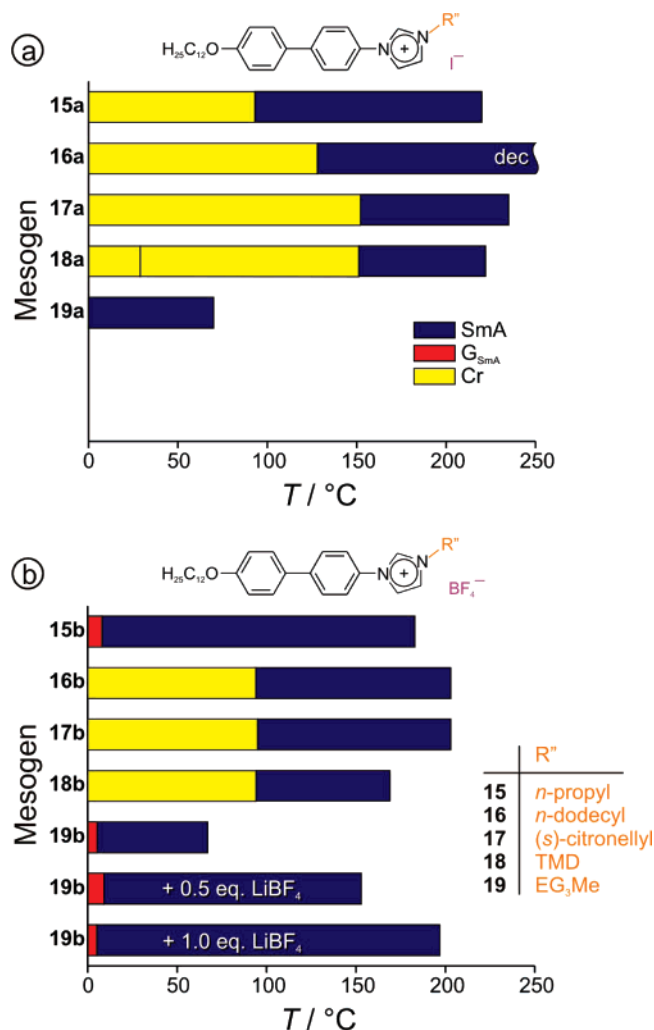


Figure 5. Mesomorphic properties of **15–19** (generic structures shown above the diagrams): (a) Iodide salts and (b) BF_4^- salts. Note that **16a** starts decomposing above 250 °C. Upon fast heating a clearing temperature of approximately 270 °C was observed in microscopy experiments.

clearing temperatures and promotes smectic phases. We limited ourselves to short (C_3) or long (C_{12}) linear tails and investigated introduction of multiple small branches by using racemic (3,7,11-trimethyldodecyl) and chiral ((S)-citronellyl) tails. We also prepared an oligo(ethyleneglycol) derivative to study the interactions between the imidazolium salt and a polar tail. The synthesis and subsequent ion-exchange reactions yielded both iodide and BF_4^- salts for parallel analysis. The transition temperatures are summarized in Figure 5. Latent heat values for the BF_4^- salts are shown in Table 3.

ILCs with long aliphatic tails **16–18** show very similar mesomorphic properties, both in transition temperatures and latent heat. The presence of small branches has limited influence on the mesophase stability. In other reports on non-ionic liquid crystals, it has been found that the use of the trimethyldodecyl tail, with disordered methyl groups, widens the mesophases by suppression of crystallization. It has also been reported that the chiral branches in the citronellyl group cause an increase in the melting temperature. However, both modifications have limited effects in our prepared series of ILCs. The phase behavior of the BF_4^- salts is comparable to that of the corresponding iodide salts. Further details of the influence of the counterion are discussed later in Series 2.

The mesogen carrying the short propyl tail (**15**), displays a different behavior. Although the transition temperature of **15** is in the range of **16–18**, the latent heat at the clearing point is much lower, indicating a lower degree of organization in the SmA phase. Interestingly, upon ion exchange from I^- to BF_4^- crystallization is suppressed, and a very wide mesophase is formed, ranging from room temperature to nearly 200 °C.

The glycol-functionalized mesogens are very different from other members of the series. The transition temperatures are very low: **19a** shows glass transition at -1°C , **19b** melts at 8°C , and both show clearing temperatures that are 100 °C lower than those of the rest of the series. The deviant behavior of **19** is likely associated with the presence of dipolar interactions between the imidazolium ion and the oligoglycol tail. When one equivalent of LiBF_4 is added to **19b**, the clearing temperature jumps up to values similar to those of the other members of the series. We suggest that Li^+ ions in the mixture compete with the imidazolium group in complexing the glycol tails. This allows for a more rod-shaped conformation of the mesogen, which in turn increases the clearing temperatures. This argument is in line with preliminary molecular modeling results, discussed in the Supporting Information.

The BF_4^- salts of **15–19** were subjected to XRD at temperatures throughout the SmA phase. Characteristic SmA patterns were observed in all cases with a strong sharp fundamental layer reflection d_{001} and diffuse reflections in the wide-angle region. The layer spacings, obtained after fitting the (001) reflections, are shown in Figure 6. Materials with long aliphatic tails **16b**, **17b**, and **18b**, formed monolayers with layer spacings of the order of 3 nm. The degree of interdigitation at $0.95 T_{\text{Iso}}$ is comparable for all three compounds. Moreover, the bilayers formed by propyl-substituted **15b** are interdigitated to an extent similar to that of the monolayers formed by **16–18**. Compound **19b** with the glycol tails forms bilayers as well but shows much stronger interdigitation than any other member of the series. We attribute this behavior and the large temperature dependence of the layer spacing (15% over only 30 °C) for **19b** to the imidazolium–glycol interaction. Addition of LiBF_4 to **19a** reduces this strong temperature dependence to trends in accord with those observed for **15b**; however, the interdigitation remains.

Series 2. The Influence of the Counterion. When compared to conventional liquid crystals, ILCs have an additional parameter for mesophase manipulation: the counterion. The counterion has a large effect on both the melting and the clearing temperatures.²² We chose to investigate a small selection of counterions, including BF_4^- , PF_6^- , and ClO_4^- ions. These ions have hydrophobic tendencies, and a low sensitivity to atmospheric humidity was anticipated. The trends are mesogen dependent. However, for most materials, halides show higher clearing temperatures than the lipophilic anions PF_6^- , BF_4^- , and ClO_4^- .²²

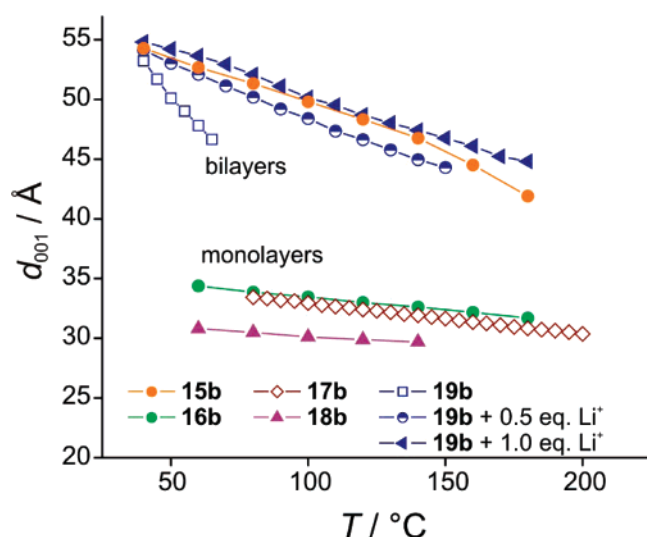
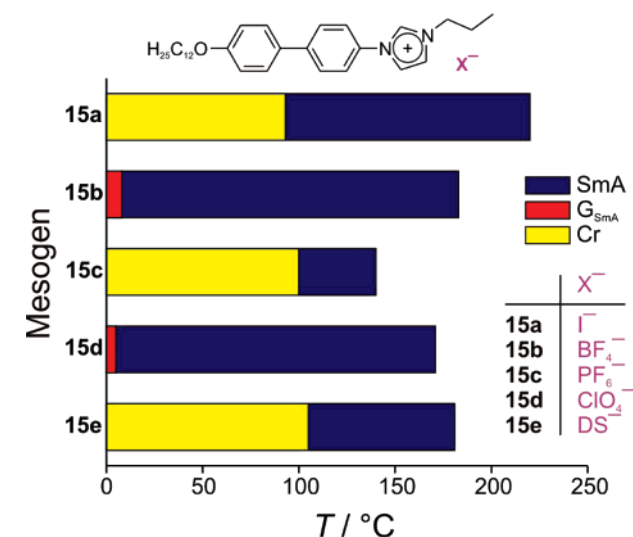
In the series **15a–d**, the clearing points decrease in the order: $\text{I}^- > \text{BF}_4^- > \text{ClO}_4^- > \text{PF}_6^-$ (Figure 7 and Table 3). In addition, we observed that the crystallization of **15b** and **15d** is suppressed, and hence, the mesophase window can be extended to room temperature to give a SmA phase width of 150 °C.

Table 4 summarizes the DSC and XRD data for **15a–15e**. The ILCs **15a–15d**, with small counterions, show strong similarities both in latent heat at the clearing temperature (the

Table 3. Latent Heat and XRD Data of *N*-Alkyl Substituent Variation

LC	R''	$\Delta H_{\text{Cr-SmA}}^a$ / kJ mol ⁻¹	$\Delta H_{\text{SmA-Iso}}^b$ / kJ mol ⁻¹	L_{calc}^c / Å	$L_{\text{XRD}}^{d,e}$ / Å	$L_{\text{XRD}}/L_{\text{calc}}^e$	
15b	<i>n</i> -propyl	—	0.6	30.5	44.5	0.73	
16b	<i>n</i> -dodecyl	13.1	3.4	41.5	31.7	0.76	
17b	3,7,11-tridodecyl	14.3	3.7	41.2	30.9	0.75	
18b	(<i>S</i>)-citronellyl	14.4	2.5	36.7	29.5	0.80	
19b	3,6,9-trioxadecyl	10.4	0.2	38.0	48.4	0.64	
19b + 0.5 equiv LiBF ₄		—	0.2	38.0	45.5	0.60	
19b + 1.0 equiv LiBF ₄		—	0.2	38.0	45.2	0.59	

^a Latent heat at the crystal to SmA transition (taken from the second heating trace). ^b Latent heat at the SmA to isotropic transition. ^c Length of the stretched molecule, determined by molecular modeling. ^d Layer spacing, determined by XRD experiments: for monolayers $L_{\text{XRD}} = d_{001}$, for bilayered materials $L_{\text{XRD}} = 1/2 \times d_{001}$. ^e L_{XRD} was determined at $T = 0.95T_{\text{Iso}}$ (after interpolation of the data).

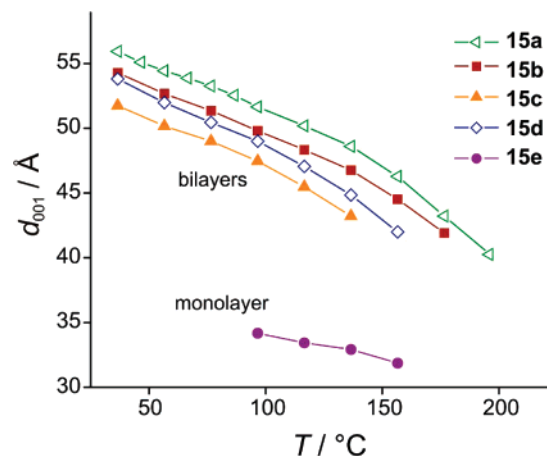
**Figure 6.** XRD-determined time dependence of the layer spacing in the SmA phase of the BF₄[−] salts of **15**–**19**. Note that **15b** and **19b** form bilayers, whereas for **16b**, **17b**, and **18b**, monolayers are observed.**Figure 7.** Mesomorphic properties of **15a**–**15e** (generic structures shown above the diagrams).

amount of SmA order lost at the transition) and their layer spacings. They form highly interdigitated SmA₂ phases and similar layer spacings with iodine being the largest ($\text{I}^- > \text{BF}_4^- > \text{PF}_6^- > \text{ClO}_4^-$). The temperature dependencies of the layer spacings (Figure 8) are nearly identical for all these materials.

Table 4. Latent Heat and XRD Data of **15a**–**15e**

LC	X [−]	$\Delta H_{\text{Cr-SmA}}^a$ / kJ mol ⁻¹	$\Delta H_{\text{SmA-Iso}}^b$ / kJ mol ⁻¹	L_{calc}^c / Å	$L_{\text{XRD}}^{d,e}$ / Å	$L_{\text{XRD}}/L_{\text{calc}}^e$	
15a	I [−]	38.8	0.6	30.5	41.0	0.67	
15b	BF ₄ [−]	—	0.6	30.5	44.4	0.73	
15c	PF ₆ [−]	31.0	0.6	30.5	45.5	0.75	
15d	ClO ₄ [−]	—	0.5	30.5	43.5	0.71	
15e	H ₂₅ C ₁₂ SO ₃ [−]	50.6	3.0	44.2	32.0	0.72	

^a Latent heat at the crystal to SmA transition (taken from the second heating trace). ^b Latent heat at the SmA to isotropic transition. ^c Length of the stretched molecule, determined by molecular modeling. ^d Layer spacing, determined by XRD experiments, for monolayers $L_{\text{XRD}} = d_{001}$, for bilayered materials $L_{\text{XRD}} = 1/2 \times d_{001}$. ^e L_{XRD} was determined at $T = 0.95T_{\text{Iso}}$ (after interpolation of the data).

**Figure 8.** Temperature dependence of the layer spacing in the SmA phase of **15a**–**e** as determined by XRD experiments. Note that only **15e** forms monolayers, while bilayers are observed for **15a**–**d**.

To contrast the small hydrophobic counterions, we also prepared a derivative with a dodecylsulfonate group **15e**, wherein the counterion bears another hydrocarbon tail. Interestingly, this material behaves completely differently from that of the other members of this series. The latent heat at the clearing transition is much larger than that of **15a**–**d**; in fact, it is nearly the same as that observed for **16b**, the dodecyl-substituted ILC. XRD experiments reveal monolayer formation for **15e**.

Series 3 and 4. The Influence of the Core Size and Lateral Substituents. In (conventional) liquid crystals, one of the driving forces for mesophase formation is excluded volume. The energy of a rigid anisotropic body can be decreased by aligning with

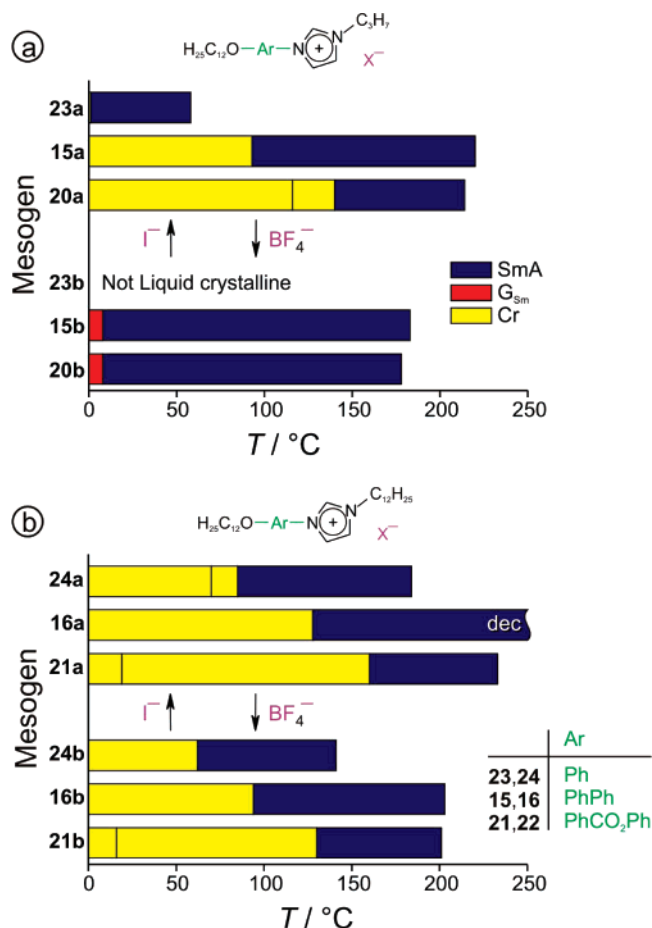


Figure 9. Mesomorphic properties of Series 3 (ILCs with different cores): (a) series R'' = propyl, X⁻ = I⁻ (top) and X⁻ = BF₄⁻ (bottom); (b) same series with R'' = dodecyl and X⁻ = I⁻ (top) and X⁻ = BF₄⁻ (bottom). The generic structures are shown above the diagram.

its environment. This explains why liquid crystal phases are observed predominantly in anisometric molecules. Aspect ratio has a major effect on the phase stability as well as the type of mesophase. Lateral substitution of the core with (small) side groups decreases the aspect ratio and often prevents dense molecular packing in the mesophase, which usually leads to decreased order in the mesophase and lower clearing temperatures.

We prepared ILCs with different core sizes and decided to use the imidazolium group for lateral substitution in order to (i) facilitate synthesis, as 2-substituted imidazoles are commercially available or readily accessible and (ii) improve stability since it removes the potentially labile proton on the imidazolium ring.

Figure 9 compares the transition temperatures of four groups of ILCs with cores differentially substituted with: (a) propyl substituents and (b) dodecyl substituents. The results of the I⁻ salts are in the top of the diagrams, and those of the BF₄⁻ salts are at the bottom. An increase in the core size by the introduction of an ester group between the two phenyl rings results in a decreased range of SmA stability due to an increase in the melting temperatures. In addition, all of the prepared esters display polymorphism at low temperatures with up to three (soft) crystal phases. A decreased core size obtained by omitting one of the phenyl rings has a large effect on the mesomorphic properties. For the propyl-substituted material, **23a** (I⁻ salt), the

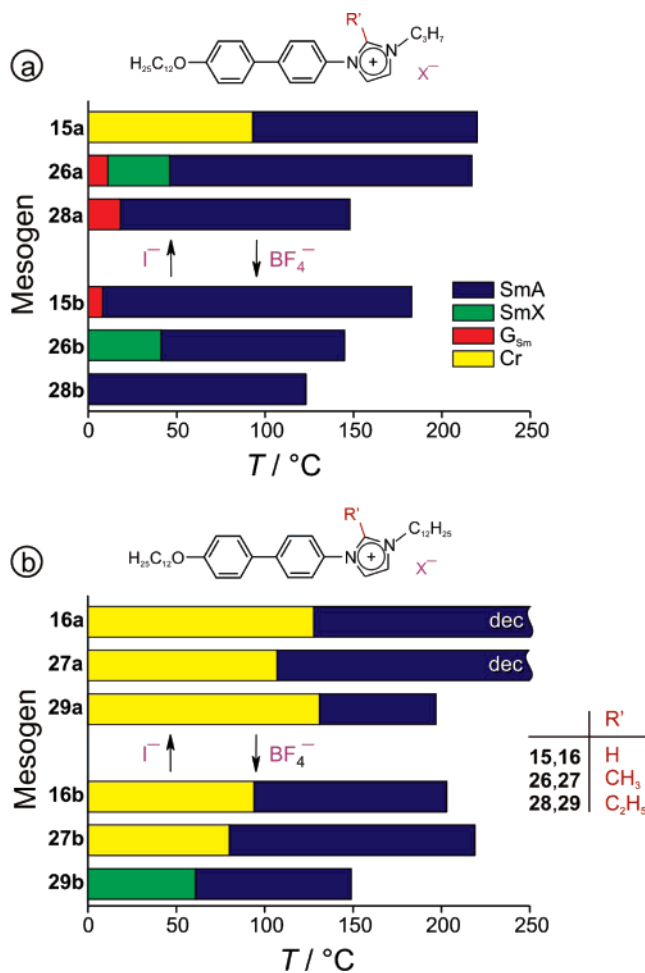


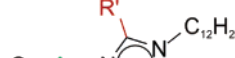
Figure 10. Mesomorphic properties of series 4 (ILCs with lateral substituents): (a) series R'' = propyl, X⁻ = I⁻ (top) and X⁻ = BF₄⁻ (bottom); (b) same series with R'' = dodecyl and X⁻ = I⁻ (top) and X⁻ = BF₄⁻ (bottom). The generic structures are shown in the diagram.

clearing temperature drops significantly to 57 °C and the corresponding BF₄⁻ salt does not exhibit liquid crystalline properties. By increasing the tail length from propyl to dodecyl **24** (or trimethyldodecyl, see Supporting Information) stable mesophases are obtained, but the clearing temperatures remain much lower than those of **16**.

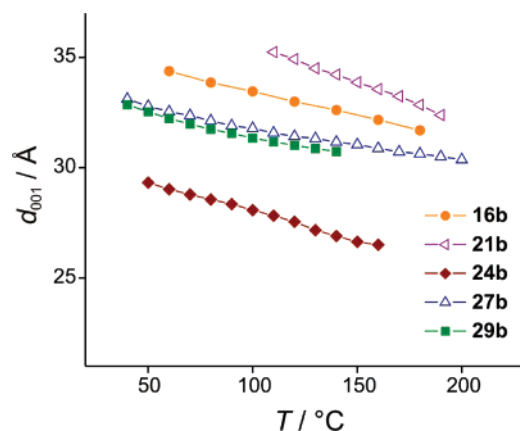
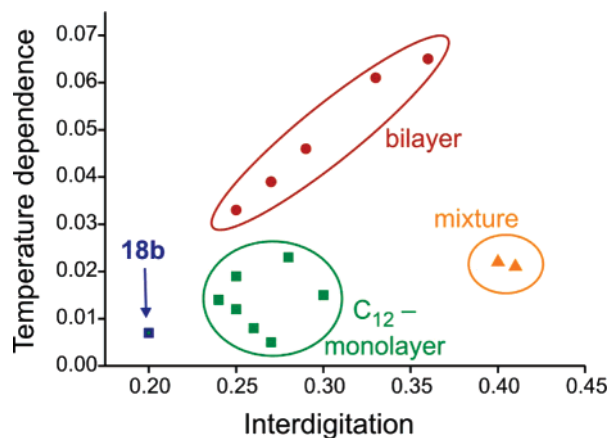
The influence of lateral core substitutions is shown in Figure 10. The sterically undemanding methyl group has limited effect on the phase stability, and small differences relative to the unsubstituted mesogens **15** and **16** are observed. As the size of the lateral group increases, the mesophase and crystal phase stabilities are considerably decreased, and **28b** displays a *T_g* of −2 °C. In other cases, such as **29b**, the suppression of crystallization by the ethyl group allows for the formation of other smectic mesophases. We also prepared larger *n*-pentyl and phenyl side groups, but for these materials no mesomorphic properties were observed. The latent heat values at the clearing transitions and the XRD results of the BF₄⁻ salts are summarized in Table 5.

Temperature-dependent XRD experiments (Figure 11) show the layer spacing of the ILCs from series 3 and 4 as a function of temperature. As expected, the observed layer spacings are largest for the extended core material **20** and smallest for the shortened **23**. When compared to their molecular length (Table 4), the extent of interdigitation is largely mesogen independent.

Table 5. Latent Heat and XRD Data of Series 3 and 4

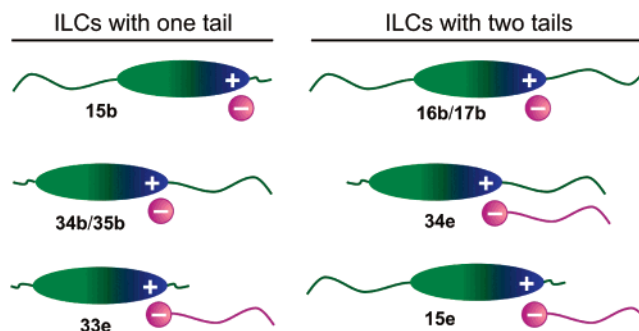
							
LC	core (Ar)	R'	$\Delta H_{\text{Cr-SmA}}^a/\text{kJ mol}^{-1}$	$\Delta H_{\text{SmA-Iso}}^b/\text{kJ mol}^{-1}$	$L_{\text{calc}}^c/\text{\AA}$	$L_{\text{XR}}^d/\text{\AA}$	$L_{\text{XR}}/L_{\text{calc}}^e$
15b	PhPh	H	13.1	3.4	41.5	31.7	0.76
20b	PhCO ₂ Ph	H	40.3	3.8	44.0	32.9	0.75
23b	Ph	H	7.5	3.0	37.5	26.4	0.70
26b	PhPh	CH ₃	41.8	3.2	41.5	30.5	0.73
28b	PhPh	C ₂ H ₅	0.7 ^f	1.6	41.5	30.9	0.74
30b	PhPh	<i>n</i> -C ₅ H ₁₁	not mesomorphic				
32b	PhPh	Ph	not mesomorphic				

^a Latent heat at the crystal to SmA transition (taken from the second heating trace). ^b Latent heat at the SmA to isotropic transition. ^c Length of the stretched molecule, determined by molecular modeling. ^d Layer spacing, determined by XRD experiments, for monolayers $L_{\text{XR}} = d_{001}$, for bilayered materials $L_{\text{XR}} = 1/2 \times d_{001}$. ^e L_{XR} was determined at $T = 0.95T_{\text{Iso}}$ (after interpolation of the data). ^f ΔH at SmX to SmA transition.

**Figure 11.** Temperature dependence of the layer spacing of the monolayer forming series 3 and 4 (dodecyl-substituted materials only).**Figure 12.** Temperature dependence of the layer spacing plotted against the degree of interdigitation. The equations defining these quantities are given in the text. For convenience, points are grouped together for the 19b/LiBF₄ mixture, 18b (C₈-citronellyl tail), the bilayer SmA phases of 15a–d and 19b and the C₁₂-substituted monolayer SmA phases of 15e, 16b, 17b, 21b, 24b, 27b, and 29b.

Laterally substituted mesogens **26** and **28** display a similar layer spacing and degree of interdigitation as the parent **16**.

When comparing the XRD results between different series of ILCs, we identified two important variables: the degree of interdigitation, defined as $1 - \{L_{\text{XRD}}(T = 0.95T_{\text{Iso}})\}/\{L_{\text{calc}}\}$, and the temperature dependence of the layer spacing $\{L_{\text{XRD}}(T = 0.90T_{\text{Iso}}) - L_{\text{XRD}}(T = 0.95T_{\text{Iso}})\}/\{L_{\text{calc}}\}$, determined over a small temperature window (with T/K). Figure 12 shows all materials for which XRD data was collected in a master plot.

**Figure 13.** Schematic representation of materials with one or two tails.

The monolayer SmA phases formed by the C₁₂-substituted mesogens are grouped together in the bottom of the plot. They are characterized by interdigitations of 25–30% of the calculated molecular length with relatively low-temperature dependence. The citronellyl derivative **18b** shows similar behavior, albeit interdigitation is slightly reduced. The temperature dependence of the bilayered systems, however, is significantly larger. The presence of the Li⁺ ions in the mixtures of **19b** with LiBF₄ causes interdigitation to increase but also results in decreased temperature dependence as compared to the other bilayer structures.

Series 5: Influence of the Position of the Aliphatic Tails.

Considering that **15b** and **34b** are isomers, we anticipated comparable mesomorphic properties. Similarly, **35b**, in which the dodecyl tail is replaced by the trimethyldodecyl tail, was expected to show behavior comparable to that of **15b**, the parent material. However, the liquid crystalline properties for this series of materials were found to be very different.

We have investigated the effect of the substitution pattern with one or two long (C₁₂) tails on the mesogenic core and the surfactant anion. As the cationic charge in the mesogenic core creates highly asymmetric ILCs, the influence of the tail substitution pattern on the mesophase behavior is substantial. Figure 13 schematically depicts the materials investigated, and their mesophase behavior is summarized in Figure 14.

Mixtures of Ionic Liquid Crystals. Mixtures of liquid crystals are widely used in commercial applications. This approach eliminates the need for design and synthesis of a mesogen with all desired properties (which possibly may not exist). An additional advantage of mixtures is that crystallization is often suppressed and mesophases can be stable at lower temperatures. To investigate the mixing behavior of our newly

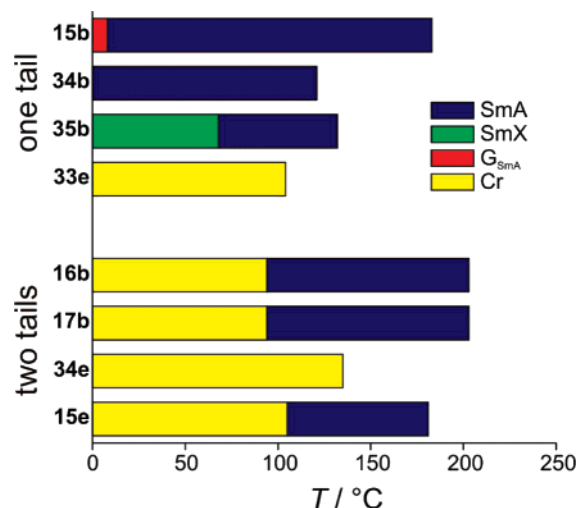


Figure 14. Comparison of the mesomorphic properties of ILCs with one and two (branched) C_{12} tails. The structures are represented schematically in Figure 13.

prepared ILCs, we prepared binary and ternary mixtures (Table 6) that were investigated by DSC and OPM.

Contact samples of two different mesogens were prepared by allowing two small drops of ILC in the isotropic phase to mix under a cover slip. The interface between the two materials was studied by OPM by varying the temperature. Contact samples of structurally similar mesogens always showed complete (linear) miscibility of the two components. Interesting behavior was observed for the contact sample prepared from **15b** and **34b** (isomers with a different position of the propyl tail). Both materials mixed homogeneously in the isotropic phase, but the mixture did not permit mesophase formation. The microscope image showed two different textures of the mesophases of both materials separated by an isotropic region as shown in Figure 15a. Compound **34b** showed a clear, focal, conical texture, while **15b** showed a grainy texture with a tendency for homeotropic alignment in the bulk of the material. The isotropic region did not disappear upon cooling to room temperature. Similarly, the SmA phases of compounds **26b** and **36b**, both substituted with methyl groups on the tail and the core, respectively, are immiscible in the SmA phase. The two (different) textures are separated by an isotropic region (Figure 15b), that reduced in size when cooling the sample to room temperature, but never disappeared. Annealing the structure (for multiple days) gave rise to complete phase separation into the two (smectic) components.

Mesogens **20a** and **23a** (same substitution pattern, but different core size) are an example of a completely miscible system. In the contact sample (Figure 15c), the bulk of **20a** is

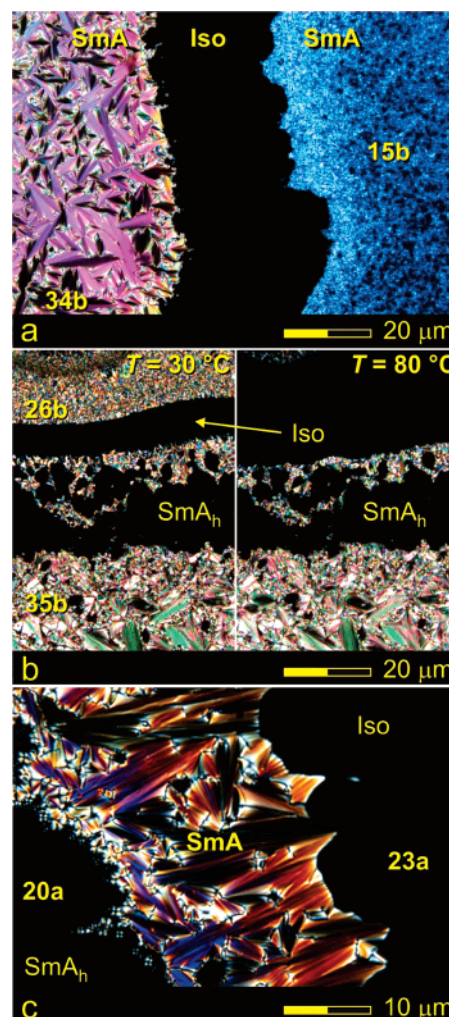


Figure 15. Contact samples of (a) **15b/34b** at 125 °C and (b) **26b/35b** at 80 °C (right) and 30 °C (left). Both pictures show immiscibility of the pairs of SmA mesogens. Mesogens **34b** and **35b** show a focal conic texture; **15b** and **26b** a grainy texture or homeotropic on cooling. The dark homeotropic SmA areas are labeled SmA_h. This is not a separate phase assignment but is used to distinguish the black texture from the isotropic areas. The area in between the SmA phases is isotropic. (c) Mixture **20a/23a** at 60 °C: **20a** is homeotropically aligned (bottom left) and at the interface with **23a** a focal conic texture appears. All pictures were taken between crossed polarizers.

aligned homeotropically. On cooling, the SmA interface slowly shifts toward the bulk of **23a**. At the interface, a classical focal conic texture appears. The picture in Figure 15c was recorded just above the clearing temperature of **23a** and further cooling of this sample resulted in the formation of a focal conic texture in the bulk of **23a**.

Table 6. Composition and Phase Behavior of Mixtures of ILCs

mixture	composition (molar fractions)			miscibility ^a	phase behavior ^{b,c} $T / ^\circ\text{C}$ and $(\Delta H / \text{kJ mol}^{-1})$	$\langle M \rangle / \text{g mol}^{-1}$
I	15a (0.501)	34a (0.499)	—	i	n/a	n/a
II	15b (0.502)	34b (0.498)	—	i	n/a	n/a
III	26b (0.500)	35b (0.500)	—	i	n/a	n/a
IV	20a (0.477)	23a (0.523)	—	m	G _{SmA} 14 SmA 132 (0.4) Iso	593.6
V	16a (0.337)	21a (0.340)	24a (0.323)	m	Cr 127 (5.7) SmA 216 (2.6) Iso	717.0
VI	20a (0.336)	31a (0.332)	35a (0.332)	m	G _{SmA} 6 SmA 164 (1.7) Iso	667.2
VII	20b (0.331)	24b (0.331)	34b (0.338)	m	Cr 21 (broad) SmA 83 (0.7) Iso	577.9

^a i = immiscible, m = miscible. ^b G_{SmA} = glass with SmA phase frozen in, SmA = smectic A, Iso = isotropic. ^c To determine the latent heat in kJ mol^{-1} , the average molecular weight calculated from the molecular weight of the constituents, weighted by the mol fraction x : $\langle M \rangle = \sum_i M_i x_i$.

Table 7. Observed Clearing Temperatures and Latent Heat, Compared to Calculated Values

mixture	$T_{\text{iso,exp}}/^\circ\text{C}$	$\Delta H_{\text{iso,exp}}/\text{kJ mol}^{-1}$	$\langle T_{\text{iso}} \rangle^a/^\circ\text{C}$	$\langle \Delta H_{\text{iso}} \rangle^a/\text{kJ mol}^{-1}$
IV	132	0.4	132	1.0
V	216	2.6	230 ^b	4.1 ^b
VI	154	1.7	151 ^c	2.4 ^c
VII	83	0.7	146	1.9

^a To predict the transition temperatures and the latent heat, we used the weighted average of the components: $\langle T_{\text{iso}} \rangle = \sum_i T_{\text{iso},i} x_i$ and $\langle \Delta H_{\text{iso}} \rangle = \sum_i \Delta H_{\text{iso},i} x_i$. ^b Estimated values for **16a**: $T_{\text{iso}} = 270^\circ\text{C}$, $\Delta H_{\text{iso}} = 4 \text{ kJ mol}^{-1}$. ^c Estimated values for **31a**: $T_{\text{iso}} = 50^\circ\text{C}$, $\Delta H_{\text{iso}} = 0.3 \text{ kJ mol}^{-1}$.

Discrete binary and ternary mixtures (Table 6) were analyzed by DSC. Immiscible samples (mixtures **I–III**) showed DSC traces with multiple broad peaks. DSC traces of miscible samples, as judged by OPM (mixtures **IV–VII**), displayed well-defined SmA to isotropic transitions that are slightly broadened with respect to the pure compounds. Some of the miscible samples showed partial crystallization after extended periods at room temperature.

Table 7 shows the clearing temperatures and corresponding latent heat values of mixtures **IV–VII**, compared to the average values (weighted by mole fractions) of the separate components. The close correspondence of the clearing temperatures of mixtures **IV** and **V** indicates nearly linear miscibility and thus, close to ideal behavior. Observed values of the latent heat at the clearing temperature are lower than the calculated average values. This can be readily understood because a SmA phase containing a mixture of mesogens of different dimensions would be expected to show reduced order.

On the basis of OPM studies, we found that binary mixture **IV** shows complete suppression of crystallization and the viscosity of the sample was judged (qualitatively) to be lower than that of the pure components. The sample could easily be sheared in the SmA phase at 50°C , a temperature 80°C below the clearing temperature.

We were surprised to find that mixture **VI**, which contains the non-liquid crystalline **31a** and is very similar to the immiscible mixture **III**, displayed liquid crystal properties. In fact, for mixture **VI** the experimental data is very close to the average values of the components. Mixture **VII** with similar components shows a much lower clearing temperature than would be expected. Clearly, mixing ILCs can be successful in creating new properties.

Conclusions

Liquid crystals with ionic rigid cores constitute a relatively new class of materials in which self-organization and macroscopic anisotropy are imparted to ionic liquids. The anisotropic properties that these materials offer may find applications in functional devices, such as photovoltaic fuel cells, or as a

templating medium for the electrosynthesis of materials. Despite the potential impact, this is the first extensive parameter study to be performed on these types of mesogens.

Using newly developed aryl-amination chemistry, we have prepared a series of ILCs wherein the charged (imidazolium) group has been incorporated in the rigid part of the mesogen. The increased core size, as anticipated, has a positive effect on the order parameter of these new materials when compared to simple long-chain 1-alkyl-3-methylimidazolium salts. This mesogenic core allowed us to conduct a full investigation of how the structural parameters influence mesophase formation. Investigated parameters included: (i) the size and nature (branching effects) of the aliphatic tails and the substitution of those tails with corresponding ethylene glycol tails, (ii) the size of the mesogenic core, (iii) lateral substitution on the mesogenic core, and (iv) the nature of the counterion.

In summary, our results indicate that mesogens with a larger core display more stable SmA phases (higher clearing temperatures), but also higher melting temperatures. The latter can be reduced by introducing small laterally attached substituents. When lateral substituents become too bulky, the mesogenic properties are lost. Mesogens substituted with two long flexible aliphatic tails form interdigitated SmA_d phases. Branching of the tails (either in racemic or chiral form) has minimal influence on the phase behavior. Short tail substituents introduce the formation of SmA₂ phases (interdigitated bilayers). Mesogens substituted with ethyleneglycol tails show deviant behavior (reduced mesophase stability), due to the interaction of the tail with the imidazolium cation. Doping these systems with LiBF₄ stabilizes the mesophase and has the additional advantage that the Li⁺ ions can improve rates of anisotropic ion conductivity.

Mixtures of different ILCs are completely miscible in some cases, and ideal mixing behavior has been observed. The use of such mixtures offers advantages over the use of pure compounds by suppressing crystallization and giving low-viscosity SmA phases, which is important for potential applications. In other ILC mixtures incompatibility of the two SmA phases was observed, thereby indicating that additional structural investigations of the mesophases are necessary.

Acknowledgment. This work was supported by the National Science Foundation and European Union through the Marie Curie International Outgoing Fellowship of PHJK.

Supporting Information Available: Experimental details, synthesis, structural characterization, liquid crystal properties of all 47 final products and intermediates and molecular modeling results. This material is available free of charge via the Internet at <http://pubs.acs.org>.

JA075651A